Journal of Materials Chemistry A

ROYAL SOCIETY OF CHEMISTRY

PAPER

View Article Online
View Journal | View Issue

Cite this: J. Mater. Chem. A, 2025, 13, 27349

Graphene oxide lowers carbon monoxide polymerization pressure through chemical pre-compression†

Xiuyuan Li, [a] Zihuan Peng, [a] Chongwen Jiang,[a] Zhihong Huang,[a] Nan Li,*[a] Shaomin Feng,[b] Jun Zhang[b] and Changqing Jin*[b]

Received 24th April 2025
Accepted 8th July 2025

DOI: 10.1039/d5ta03235k

rsc.li/materials-a

Polymeric carbon monoxide (p-CO) is one of only a few low-Z extended solids that form under high pressure and can be recovered under ambient conditions. As an innovative carbon-based material with potential applications, its development is restricted by the harsh synthesis conditions and metastability. Motivated by the application of two-dimensional (2D) materials to facilitate reduction reactions of N_2 and CO_2, the metal-free initiators/catalysts, graphene and graphene oxide (GO), were introduced into the carbon monoxide (CO) system under high pressure to investigate their effects. Our *ab initio* theoretical study demonstrates that GO can provide chemical force to "pre-compress" the CO molecules and greatly lower the polymerization pressure from 5 GPa to 3 GPa (a 40% decrease). The catalytic mechanism analysis elucidates that GO can significantly reduce the free energy barrier for the CO dimerization reaction, which is the most challenging step in the CO polymerization process. Moreover, the introduction of GO can effectively improve the stability of p-CO *via* forming C–C bonds, H-bonds and H-transfer at the GO-CO interface. Our study presents a novel approach for achieving condensed matter under milder conditions and extends the application of 2D materials as initiators to high-pressure synthesis, contributing to their potential application as energetic materials of p-CO.

1. Introduction

Pressure is a new dimension in scientific exploration of a wide range of physical and chemical fields. As higher pressure has become attainable, various new phenomena and novel materials have emerged, and the focus of high-pressure research has progressed with time.[1] Recently, of particular interest are the low-Z extended solids produced by the high-pressure polymerization of low-Z molecules (such as CO, CO_2, N_2, O_2 and mixtures), because they have exhibited unusual properties such as superconductivity,[2] extreme hardness,[3] optically nonlinearity[4] and high energy density.[5,6] As an archetypal example of low-Z molecules, CO as well as its polymeric phases (polymeric CO, p-CO) has been the subject of intense research for several decades.[7–18] At 5 GPa and 300 K, CO can polymerize into p-CO, one of only a few low-Z extended solids that can be recovered under ambient conditions.[19] To date, p-CO has been considered as an advanced energetic material with disruptive detonation performance[20] and an ideal coating for traditional explosives.[21] However, the scaled-up synthesis of p-CO encounters great challenges due to its harsh synthesis conditions; meanwhile the metastability (photosensitive and hygroscopic) restricts its long-term storage and applications. All this drove intensive investigations focusing on reducing the synthesis pressure and improving the stability of p-CO over several decades.

In the past several decades, 2D materials have emerged as revolutionary catalysts and attracted significant research interest,[22–26] especially graphene and graphene oxide (GO). As popular metal-free 2D catalysts, they show various exceptional properties, including large surface area (2630 $m^2\ g^{-1}$),[27,28] strong chemical resistance,[29] convenient recovery of active phases,[30] good dispersibility,[31] and low-cost synthesis.[32] These properties enable graphene and GO to be utilized as initiators/catalysts in polymerization chemistry,[33–36] For example, GO can initiate the free radical polymerization of *N*-vinylpyrrolidone at 95 °C, yielding poly(*N*-vinylpyrrolidone)-grafted GO with improved conductivity (4.7 S m^{-1}).[37] Also, GO can catalyze the cationic ring-opening polymerization of ε-caprolactone and lactams at 60 °C, yielding polyesters/polyamides.[38] The broad applications of graphene and GO motivate our investigation to explore their potential roles in high-pressure synthesis, aiming to lower the pressure in p-CO synthesis. Compared with established CO polymerization promoters (H_2,[39,40] alkali metals[41] and laser irradiation[10]), graphene and GO exhibit two distinct

[a]State Key Laboratory of Explosion Science and Technology, School of Mechatronical Engineering, Beijing Institute of Technology, Beijing 100081, P. R. China. E-mail: leen04@bit.edu.cn

[b]Beijing National Laboratory for Condensed Matter Physics, Institute of Physics, Chinese Academy of Sciences, Beijing 100190, P. R. China. E-mail: jin@iphy.ac.cn

† Electronic supplementary information (ESI) available. See DOI: https://doi.org/10.1039/d5ta03235k

advantages. Firstly, as chemically stable solid-phase raw materials, graphene and GO offer superior accessibility and simplified synthetic protocols of p-CO. Secondly, when graphene and GO are mixed with p-CO, the inherent electrical, thermal, and mechanical properties of graphene and GO could be partially imparted to the composites,[33] endowing p-CO/graphene and p-CO/GO with exceptional properties.

In this study, a comprehensive theoretical investigation on the high-pressure polymerization of CO/graphene and CO/GO systems was carried out. The stepwise compressions simulated by *ab initio* molecular dynamics (AIMD) revealed the polymerization initiator roles of graphene and GO with spatial confinement and catalytic effects. Then slow-growth simulations, density functional theory (DFT) calculations and electronic wavefunction analysis were used to investigate the catalytic mechanisms. Structural analysis revealed the stabilizing effects of graphene and GO on p-CO. The present work not only paves the way for the synthesis of condensed matters under milder conditions, but also offers new insights into the application of 2D carbon-based materials as initiators under high pressure.

2. Computational methods

The graphene molecule of 32 atoms was constructed based on the graphene crystal structure in the Cambridge Crystallographic Data Centre (CCDC), and the GO molecule of 51 atoms was acquired from ref. 32 with 8 hydroxyl groups and 3 epoxide functions. The two molecules have both zigzag and armchair edges, which agree well with experiments.[42,43] To maintain the intrinsic reactivity of these edges, the unsaturated valence electrons were preserved without additional passivation or modification. Also, according to ref. 32, the edge functionalization with carboxylic functions for GO was discarded. To balance the computational efficiency with simulation accuracy and comprehensively simulate all the possible reactions between graphene/GO and CO, the initial models of the CO/graphene or the CO/GO systems were generated by placing 150 CO molecules and 1 graphene or GO molecule into a cubic box with a side length of 20 Å using the Packmol program.[44] According to the CO phase diagram,[11] CO at high pressure and 300 K is always disordered, and thus the CO molecules in the initial models were randomly packed. The density values of CO/graphene and CO/GO initial models are 0.95 and 0.99 g cm^{-3}, respectively, which are close to that of a pure CO system at 2 GPa/300 K (1.06 g cm^{-3} from AIMD simulations[45]) to ensure effective initial equilibrium.

Geometry optimizations, AIMD simulations and slow-growth[45] simulations were performed by the CP2K 8.2 package[46] using Gaussian and plane-waves (GPW) approach[47] at the GTH-PBE/DZVP-MOLOPT-SR-GTH[48] level of theory with a cutoff of 800 Ry. The Bohn–Oppenheimer approximation[49] was applied for all the simulations. The CO/graphene and the CO/GO systems were optimized at 2 GPa before the simulations. The AIMD simulations were performed in the NPT ensemble using the DFT-D3 method,[50] the canonical sampling through velocity rescaling (CSVR) thermostat[51] and the Martyna–Tobias–Klein (MTK) barostat[52] with a time step of 1 fs. Each system was initially equilibrated at 2 GPa/300 K, followed by sequential compression to 3, 4, 5, 7, and 10 GPa, with a final equilibration and optimization at 0 GPa. The simulations under 2–4 GPa were performed to investigate the catalytic effects of graphene and GO. The simulations under 10 GPa were performed to obtain fully polymerized p-CO/graphene and p-CO/GO. The simulations under 0 GPa were performed to obtain recovered p-CO/graphene and p-CO/GO. The CO/graphene and the CO/GO systems were respectively equilibrated for 5 ps and 8 ps at each pressure. As for the slow-growth simulations, the representative frames in the equilibrated trajectories at 2 GPa/300 K of AIMD simulations were selected as the input. Taking the C–C distance as the collective variable, the distances were changed slowly with a rate of -0.0004 Å fs^{-1} from the initial distance of 3.0 Å. Each slow-growth simulation was performed for 4 ps. The free energy profiles were calculated through integrating the gradients of potential energy. All the systems were treated with the unrestricted Kohn–Sham (UKS) approach.

To elucidate the influence of π-conjugation on CO adsorption, two simplified models (namely "conjugated" and "non-conjugated") were constructed for electronic structure analysis. By selectively cleaving several C–C bonds, the "non-conjugated" model was obtained from the CO/GO structure under 2 GPa (Fig. 1a), and the "conjugated" model was obtained from the CO/graphene structure under 2 GPa (Fig. 1b). Both models have 3 absorbed CO molecules and 4 fused rings with the edges passivated by H atoms. The simplified models were optimized by ORCA 6.0,[53–55] at the B3LYP-D3/def2-TZVP(-f) level of theory[56–58] with the unrestricted Kohn–Sham (UKS) approach. No imaginary vibrational frequency was found. The single point calculations were performed at the wB97M-V/def2-TZVP level of theory.[59] The same computational protocol was also applied to evaluated the reaction energy for H-transfer between GO and p-CO. Based on the truncated models of p-CO and GO from recovered p-CO/GO, the H-bond energy was calculated by the symmetry adapted perturbation theory (SAPT)[60] implemented in

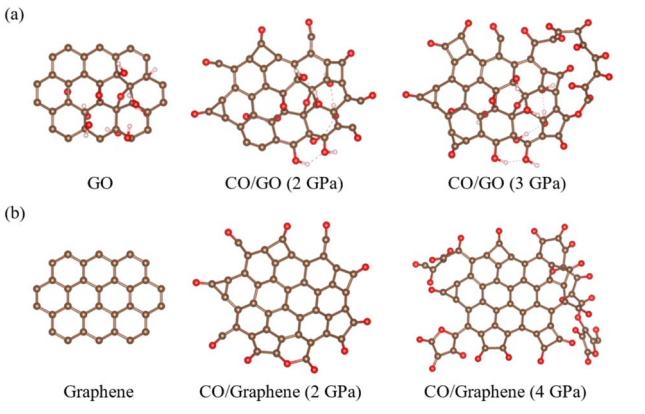

Fig. 1 Structures of graphene and GO under different pressures, where the brown, red and white balls denote C, O and H atoms, respectively. (a) Graphene in the CO/graphene system before simulations, under 2 GPa and 3 GPa, respectively. (b) GO in the CO/GO system before simulations, under 2 GPa and 3 GPa, respectively.

the PSI4 1.3.2 code[61] at the sSAPT0/jun-cc-pVDZ[62] level of theory. Multiwfn 3.8[63] was applied to prepare the input files of CP2K and ORCA programs and calculate the Mayer bond order (MBO),[64] σ-MBO, π-MBO and π electron density.[65] The VESTA 3.5.7[66] and VMD 1.9.3[67] programs were used to visualize the structure data and trajectories.

3. Results and discussion

After the optimizations under 2 GPa, the initial models of CO/graphene and CO/GO were condensed to 1.46 and 1.48 g cm^{-3}, respectively. Then the AIMD simulations of stepwise compression were performed. The simulations at 2 GPa revealed that CO molecules were adsorbed on the edges of graphene and GO. The density values of CO between the graphene and GO layers are 1.611 and 1.485 g cm^{-3}, respectively higher than that of the pure CO system of 1.358 g cm^{-3}. Similar spatial confinement effects of 2D graphene-based materials were observed for other systems.[68] When the pressure reached 3 GPa, for the CO/GO system, the adsorbed CO forms C–C bonds with free CO and produces a C_2O_2 dimer, which further grew through the successive formation of C–C bonds with adjacent CO to generate adsorbed C_nO_n chains, as shown in Fig. 1a. A similar polymerization process occurred for the CO/graphene system when the pressure reached 4 GPa, as shown in Fig. 1b. According to our previous simulations,[69] the transition pressure from CO to p-CO is 5 GPa, which is significantly higher than 3 GPa observed in the CO/GO system, suggesting that GO and graphene likely serve as effective initiators for p-CO polymerization.

During the polymerization from CO to p-CO, the dimerization of CO represents the most challenging and rate controlling step as it is the only reaction step where no radical is involved.[69] Therefore, it was speculated that both graphene and graphene oxide (GO) can catalyze the dimerization reaction to promote the formation of p-CO at lower pressure. To prove this point, the slow-growth simulations were performed to calculate the evolution of free energy for the dimerization reactions in CO, CO/graphene and CO/GO systems, as shown in Fig. 2. In each system, the collective variable (CV) is defined as the C–C distance, as illustrated in Fig. 2a. The dimerization reactions were simulated by shortening the CVs from 3.00 Å to 1.40 Å. According to the free energy profiles in Fig. 2b, the pristine CO system has the highest free energy barrier (91.46 kJ mol^{-1}), followed by the CO/graphene system (69.31 kJ mol^{-1}), while the CO/GO system shows the lowest barrier (52.81 kJ mol^{-1}). These results indicate that both graphene and GO can catalyze the dimerization reactions of adsorbed CO. Meanwhile, the C–C distances corresponding to the free energy maximum for the CO/graphene and the CO/GO systems are ~1.90 Å, related to the transition states for dimerization reactions (Fig. S2†). That distance in the pristine CO system is ~1.60 Å, and there is no corresponding transition state, indicating evident differences in the reaction pathways among these systems. According to the simulation trajectories, when the CV reaches ~1.60 Å, free CO molecules in the CO system successively participate in the formation of adsorbed C_nO_n chains, leading to a decrease in free

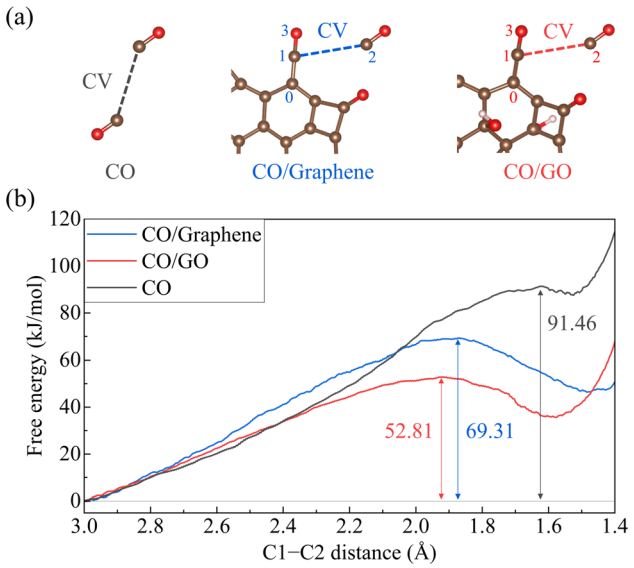

Fig. 2 The dimerization reactions of CO simulated by the slow-growth method. (a) CVs of the CO, CO/graphene and CO/GO systems (C–C distance), where the brown, red and white balls denote C, O and H atoms, respectively. (b) Free energy as a function of CVs.

energy. However, both CO/graphene and CO/GO systems exhibit earlier reaction initiation at a longer CV of ~1.90 Å, suggesting that both graphene and GO can facilitate the chain elongation reactions of adsorbed CO ($OC^{\bullet}$–$(C{=}O)_{n-1}$–$C^{\bullet}O$ + CO → $OC^{\bullet}$–$(C{=}O)_n$–$C^{\bullet}O$).

To further investigate the catalytic mechanisms of graphene and GO, structural analysis was performed based on the simulation trajectories. During the dimerization reaction in the CO/graphene and the CO/GO systems, the evolution of chemical bonds with respect to the CV is shown in Fig. 3. Herein, C1O3 is the CO molecule adsorbed on the edges of graphene or GO, C0 is the adsorption site of graphene or GO, and the C1–C2 distance is the CV. When the CV is 3.00 Å, the C0–C1 bond length (~1.35 Å) in both systems is close to the typical C=C

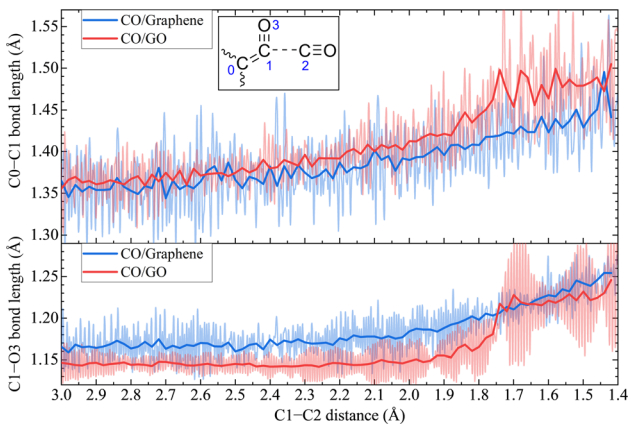

Fig. 3 Evolution of corresponding chemical bonds with respect to the CV (the C1–C2 distance) during the dimerization reaction in the CO/graphene and the CO/GO systems.

bond length (1.35 Å), and the C1–O3 bond length (~1.15 Å) is close to the typical C≡O bond length (1.15 Å). When the CV decreases to 1.40 Å, the C0–C1 bond length in both systems extends to 1.45–1.50 Å, close to the typical C–C bond length (1.52 Å), while the C1–O3 bond length extends to 1.25 Å, close to the typical C=O bond length (1.21 Å). Here, the typical bond lengths were from our previous simulations.[69] In a word, during the dimerization reaction, the adsorbed C=C bond between C0 and C1 transforms into a C–C bond, while the C≡O bond of C1O3 transforms into a C=O bond. More importantly, in the CO/graphene system, the average bond length between C0 and C1 is always longer, indicating that the adsorbed C=C bond is relatively weaker. As a result, the transformation of the adsorbed C=C bond is easier, accounting for the lower free energy barrier for the dimerization reaction. Although the average length of the C1–O3 bond in the CO/GO system is smaller than that in the CO/graphene system, which is unfavorable for the transformation of C1O3 from the C≡O bond into a C=O bond, the extension of the C1–O3 bond length (0.02 Å) during the dimerization process (the CV from 3.0 Å to 1.9 Å) is much smaller than that of the C0–C1 bond (0.05 Å). These results suggest that the C0–C1 bond plays a predominant role in governing the free energy evolution, whereas the C1–O3 bond exhibits a negligible influence on the free energy.

To elucidate the superior catalytic performance of GO over graphene, a comprehensive analysis of their electronic properties was conducted on two simplified models (namely "conjugated" and "non-conjugated"), as shown in Fig. 4. The fundamental distinction between graphene and GO in catalyzing the CO dimerization reaction primarily resides in the presence or absence of extended π-conjugation near the adsorption sites. It is well known that graphene exhibits complete sp^2 hybridization of all carbon atoms, with their singly-occupied p_z orbitals collectively forming a delocalized/global π-conjugation,[70] which is represented by the 4 conjugated rings of the "conjugated" model (Fig. 4a). Comparatively, the structural modification of graphene oxide (GO) through the introduction of oxygen-containing functional groups (hydroxyls and epoxides) significantly alters its electronic structure. The extensive distribution of these functional groups results in a substantial proportion of sp^3-hybridized carbon atoms (at least 33%),[32] consequently causing a limited and localized π-conjugation, which is represented by the 4 non-conjugated rings of the "non-conjugated" model (Fig. 4b). A comprehensive analysis was performed on the adsorbed C=C bonds (B1 and B2) in both models (Fig. 4c–e), focusing on the length, Mayer bond order (MBO), its respective contributions from σ- and π-electrons (MBO = σ-MBO + π-MBO) and electron density. The length of B1 (1.34 Å) and B2 (1.37 Å) are in great accordance with that in the AIMD simulations under 3 GPa (CO/graphene: 1.35 Å, CO/GO: 1.36 Å, see Fig. S1†), suggesting that the AIMD trajectories are reliable. The length of B2 is 0.03 Å longer than that of B1, and its MBO is 0.19 smaller, indicating that B2 is weaker than B1. Notably, the σ-MBO of B2 is nearly the same as that of B1, but the π-MBO of B2 is 0.23 smaller, suggesting that B2 has a weaker π orbital interaction compared with B1. Further analysis of π electron density is shown in Fig. 4d–e. For the

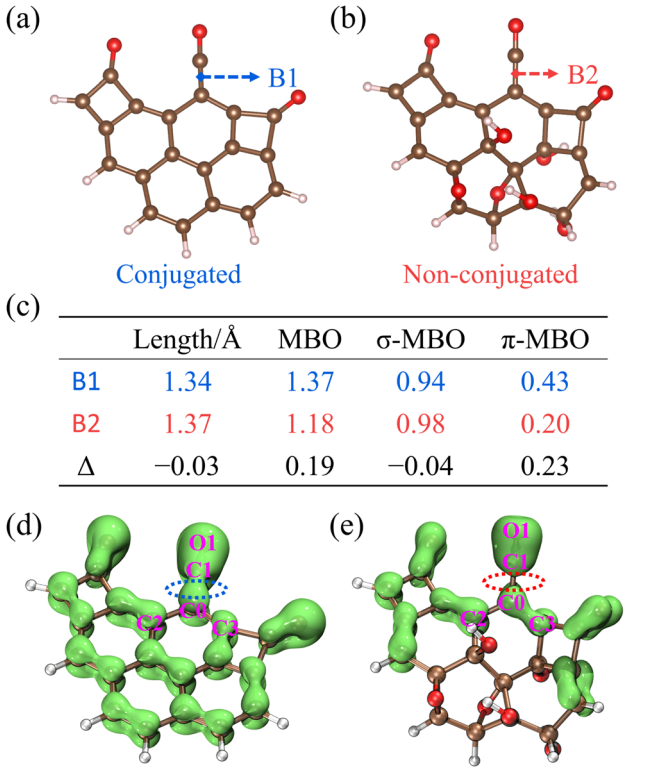

	Length/Å	MBO	σ-MBO	π-MBO
B1	1.34	1.37	0.94	0.43
B2	1.37	1.18	0.98	0.20
Δ	−0.03	0.19	−0.04	0.23

Fig. 4 Geometric and electronic structures of simplified models, where the brown, red and white balls denote C, O and H atoms, respectively. (a) The "conjugated" model based on graphene and adsorbed CO. (b) The "non-conjugated" model based on GO and adsorbed CO. (c) Length, MBO, σ MBO and π MBO of the C=C bonds of simplified models. (d) Isosurface map of π electron density of the "conjugated" model (isovalue = 0.04 a.u.). (e) Isosurface map of π electron density of the "non-conjugated" model (isovalue = 0.04 a.u.).

"conjugated" model (Fig. 4d), the adsorption site (C0) has a strong π-conjugation with adsorbed CO (C1O1) and a weak π-conjugation with adjacent atoms (C2 and C3) in the substrate. In contrast, for the "non-conjugated" model (Fig. 4e), a weak π-conjugation between C0 and C1O1 is revealed compared to that among C0, C2 and C3. This phenomenon can be explained by the fundamental principle of conjugated systems: when a C=C bond conjugates with more double bonds to form more delocalized π-conjugation, it tends to be longer and weaker. For example, the C=C bond length in benzene (1.391 Å)[71] is longer than that in *s-trans*-1,3-butadiene (1.338 Å).[72] Compared with graphene, the C=C bonds of GO are shorter and stronger due to the localized π-conjugation, and thus the π-conjugation among C0, C2 and C3 is stronger, forcing B2 to be weaker. As a result, the transformation from B2 to a C–C bond is easier for the "non-conjugated" model. In other words, the localized π-conjugation of GO serving as the chemical force causes a weakening of the adsorbed C=C bonds, which facilitates the dimerization reaction of adsorbed CO.

To investigate the interactions between p-CO and graphene or GO, the CO/graphene and the CO/GO systems were further compressed and recovered to 0 GPa to obtain p-CO/graphene and p-CO/GO. The polymer structures under different

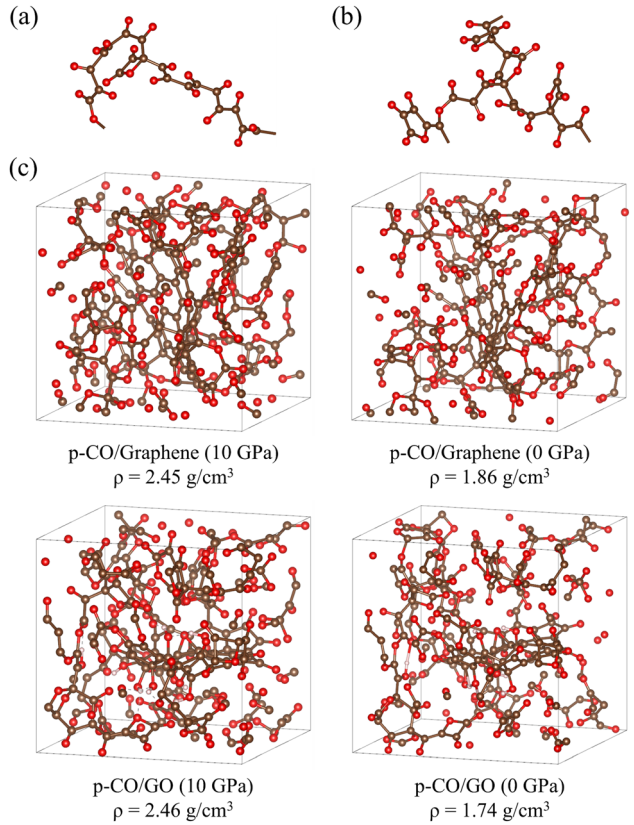

Fig. 5 Polymer structures under different pressures, where the brown, red and white balls denote C, O and H atoms, respectively. (a) A chain-like CO oligomer grows from the absorbed CO on GO under 4 GPa. (b) A CO oligomer with various rings grows from the absorbed CO on GO under 5 GPa. (c) p-CO/graphene and p-CO/GO under 10 GPa and 0 GPa.

pressures are shown in Fig. 5. Although graphene and GO can facilitate the initialization of polymerization, *i.e.*, dimerization of CO, they have little influence on the following polymerization process. The polymerization mechanism of p-CO with graphene or GO is the same as that of pure p-CO, which has been elucidated by our previous work.[69] Under 4 GPa, several chain-like CO oligomers (Fig. 5a) grow from the absorbed CO on graphene or GO through chain elongation reactions, which can be concluded as Gr/GO–$(C{=}O)_{n-1}$–C˙O + CO → Gr/GO–$(C{=}O)_n$–C˙O. Under 5 GPa, the ring closure reactions take place for the oligomers to produce diverse rings, mainly lactonic rings (Fig. 5b). Under 7 and 10 GPa, the 3D covalent network of p-CO is constructed *via* chain crosslinking reactions between the oligomers (Fig. 5c). When p-CO/graphene and p-CO/GO are decompressed to 0 GPa, the expansion of their inner cavities leads to a reduction in density, and there is no cleavage of chemical bonds. The final structures of p-CO in p-CO/graphene and p-CO/GO are similar to that of pure p-CO, which is a disordered network composed of chain-like oligomers and various rings.[69] The structure of p-CO is predominantly composed of C=O and C–C bonds (~80%) with a minor proportion of C–O and C=C bonds (~20%). Notably, the p-CO in p-CO/GO has a unique O–H bond arising from the H-transfer from GO to p-CO under high pressure. Moreover, the density of p-CO/graphene is almost the same as that of p-CO/GO under 10 GPa, because the density difference between graphene and GO is neglectable under high pressure. This density becomes higher than that of p-CO/GO under 0 GPa, because graphene has more unsaturated C atoms than GO and can form more C–C bonds with p-CO.

The interfacial structures of p-CO/graphene and p-CO/GO systems are shown in Fig. 6. Both graphene and GO are connected to p-CO through the C–C bonds on the edge (indicated by black circles), which can enhance the stability of p-CO by saturating its dangling bonds. For the p-CO/GO system, there are more interactions. Firstly, there are two intermolecular H-bonds between the hydroxyls of GO and the carbonyls of p-CO. One H-bond is indicated by the blue circle, and the bond energy is 36.27 kJ mol^{-1}, calculated on the truncated models of p-CO and GO (Fig. S3†). Secondly, during the compression simulations, H-transfer occurs twice from GO to p-CO (GO–H + p–CO˙ → GO˙ + (p–CO)–H), leading to the formation of intramolecular H-bonds in p-CO and saturation of dangling bonds. One H-transfer is indicated by the red circle, and the reaction energy is −15.06 kJ mol^{-1}, calculated on a truncated GO model and a CO molecule (Fig. S4†). It has been experimentally proven that the doping of H_2 improves the stability of p-CO,[40] and thus the H-transfer to p-CO should also do this. In conclusion, GO can stabilize p-CO *via* the formation of C–C bonds, H-bonds and H-transfer, while graphene may be less effective *via* only C–C bonds. Since the basal planes of graphene and GO are

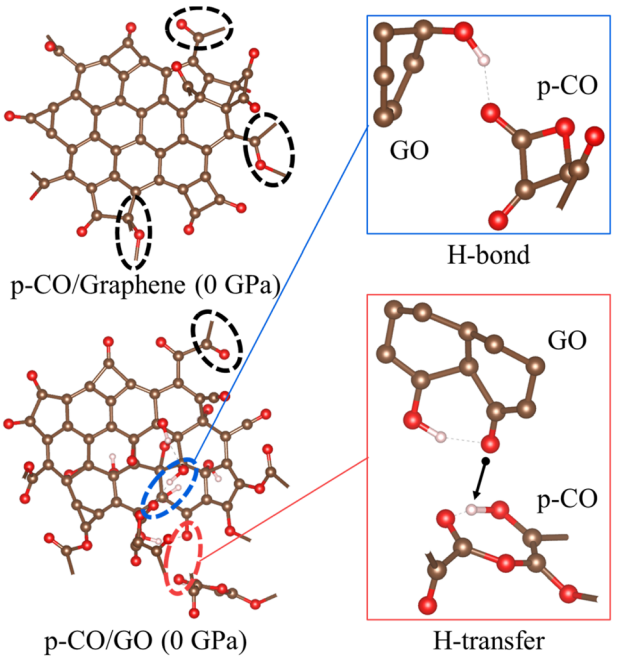

Fig. 6 Snapshots of graphene and GO in recovered p-CO/graphene and p-CO/GO, where the brown, red and white balls denote C, O and H atoms, respectively. The black circles refer to the connection between p-CO and graphene or GO, the blue circle refers to the H-bond between GO and p-CO, and the red circle refers to the H-transfer from GO to p-CO.

maintained after the compression and decompression processes, the recovered p-CO/graphene and p-CO/GO may partially possess the exceptional properties of graphene and GO.

4. Conclusions

In this study, the comprehensive calculations revealed that graphene oxide (GO) has superior catalytic effects compared to graphene in activating the CO dimerization reaction, functioning as effective initiators and lowering the CO polymerization pressure from 5 GPa to 3 GPa. The catalytic mechanism analysis demonstrates that when CO molecules are adsorbed on GO, the relatively localized π-conjugation of GO serving as the chemical force causes a weakening of the adsorbed C=C bonds, thereby facilitating the transformation from C=C bonds into C–C bonds. Then the chain elongation reactions proceed successively and induce further polymerization reactions under lower pressure. Besides, GO can effectively stabilize p-CO *via* the GO-CO interfacial interaction by forming C–C bonds, H-bonds and H-transfer. The present work provides a novel approach to polymerize the low-Z molecules under milder conditions through 2D graphene-based materials, and can be applied to the high-pressure synthesis of some emergent energetic materials like p-CO.

Data availability

The data supporting this article have been included as part of the ESI.† The structures of CO/GO and CO/graphene under different pressures are listed in Tables S1 and S2,† respectively. The structures of conjugated and non-conjugated models are listed in Tables S3 and S4,† respectively. The structures of p-CO/GO and p-CO/graphene under ambient conditions are listed in Tables S5 and S6,† respectively. Average length values of the adsorbed C=C bonds in CO/graphene and CO/GO are shown in Fig. S1.† Transition states for the dimerization reactions are shown in Fig. S2.†

Author contributions

Xiuyuan Li: conceptualization (supporting), investigation (equal) and writing – original draft (lead). Zihuan Peng: investigation (equal) and writing – original draft (supporting). Chongwen Jiang: investigation (equal) and writing – original draft (supporting). Zhihong Huang: writing – original draft (supporting). Nan Li: conceptualization (lead) and writing – review & editing (equal). Jun Zhang: writing – review & editing (equal). Shaomin Feng: writing – review & editing (equal). Changqing Jin: writing – review & editing (equal).

Conflicts of interest

There are no conflicts to declare.

References

1 M. Miao, Y. Sun, E. Zurek and H. Lin, *Nat. Rev. Chem.*, 2020, **4**, 508–527.
2 M. I. Eremets, V. V. Struzhkin, H.-k. Mao and R. J. Hemley, *Physica B*, 2003, **329**, 1312–1316.
3 S. Yamanaka, N. S. Kini, A. Kubo, S. Jida and H. Kuramoto, *J. Am. Chem. Soc.*, 2008, **130**, 4303–4309.
4 V. Iota, C. Yoo and H. Cynn, *Science*, 1999, **283**, 1510–1513.
5 M. I. Eremets, A. G. Gavriliuk, I. A. Trojan, D. A. Dzivenko and R. Boehler, *Nat. Mater.*, 2004, **3**, 558–563.
6 H.-K. Mao, C. Ji, B. Li, G. Liu and E. Gregoryanz, *Engineering*, 2020, **6**, 976–980.
7 R. Mills, D. Schiferl, A. Katz and B. Olinger, *J. Phys. Colloq.*, 1984, **45**, 187–190.
8 S. Bernard, G. L. Chiarotti, S. Scandolo and E. Tosatti, *Phys. Rev. Lett.*, 1998, **81**, 2092.
9 M. J. Lipp, W. J. Evans, B. J. Baer and C.-S. Yoo, *Nat. Mater.*, 2005, **4**, 211–215.
10 W. Evans, M. Lipp, C.-S. Yoo, H. Cynn, J. Herberg, R. Maxwell and M. Nicol, *Chem. Mater.*, 2006, **18**, 2520–2531.
11 M. Ceppatelli, A. Serdyukov, R. Bini and H. J. Jodl, *J. Phys. Chem. B*, 2009, **113**, 6652–6660.
12 S. R. Shieh, I. Jarrige, M. Wu, N. Hiraoka, J. S. Tse, Z. Mi, L. Kaci, J.-Z. Jiang and Y. Q. Cai, *Proc. Natl. Acad. Sci. U. S. A.*, 2013, **110**, 18402–18406.
13 N. Rademacher, L. Bayarjargal, W. Morgenroth, B. Winkler, J. Ciezak-Jenkins, I. G. Batyrev and V. Milman, *Chem.–Eur. J.*, 2014, **20**, 11531–11539.
14 Y.-J. Ryu, M. Kim, J. Lim, R. Dias, D. Klug and C.-S. Yoo, *J. Phys. Chem. C*, 2016, **120**, 27548–27554.
15 N. C. Dang and J. A. Ciezak-Jenkins, *J. Chem. Phys.*, 2018, **148**, 144702.
16 S. Bonev, M. Lipp, J. Crowhurst and J. McCarrick, *J. Chem. Phys.*, 2021, **155**, 054501.
17 M. Santoro, R. Bini, M. Ceppatelli, G. Garbarino, F. A. Gorelli, M. Hanfland and D. Scelta, *J. Phys. Chem. C*, 2022, **126**, 11840–11845.
18 D. Scelta, M. Ceppatelli, R. Bini, A. Pakhomova, G. Garbarino, M. Mezouar and M. Santoro, *J. Chem. Phys.*, 2023, **159**, 084501.
19 C.-S. Yoo, *Matter Radiat. Extremes*, 2020, **5**, 018202.
20 S. Sun, J. Xu, H. Gou, Z. Zhang, H. Zhang, Y. Tan and J. Sun, *ACS Appl. Mater. Interfaces*, 2021, **13**, 20718–20727.
21 W. Guan, Y. Wang, C. B. Fischer, S. Wehner, Z. Wang, J. Li, C. Wang, W. Guo and Q. Xue, *Appl. Surf. Sci.*, 2020, **505**, 144626.
22 D. Deng, K. Novoselov, Q. Fu, N. Zheng, Z. Tian and X. Bao, *Nat. Nanotechnol.*, 2016, **11**, 218–230.
23 Y. Pang, C. Su, G. Jia, L. Xu and Z. Shao, *Chem. Soc. Rev.*, 2021, **50**, 12744–12787.
24 K. Y. Ma, L. Zhang, S. Jin, Y. Wang, S. I. Yoon, H. Hwang, J. Oh, D. S. Jeong, M. Wang and S. Chatterjee, *Nature*, 2022, **606**, 88–93.
25 Z. Wu, Y. Wang, Y. Dou, L. Zhou and J. Zhu, *Nano Res. Energy.*, 2023, **2**, e9120080.

26 H. Zai, P. Yang, J. Su, R. Yin, R. Fan, Y. Wu, X. Zhu, Y. Ma, T. Zhou and W. Zhou, *Science*, 2025, **387**, 186–192.
27 A. Geim and K. Novoselov, *Nat. Mater.*, 2007, **6**, 101038.
28 R. Morales Ibarra, M. Goto, J. García-Serna and S. M. García Montes, *Carbon Lett.*, 2021, **31**, 99–105.
29 Y. Yan, W. I. Shin, H. Chen, S.-M. Lee, S. Manickam, S. Hanson, H. Zhao, E. Lester, T. Wu and C. H. Pang, *Carbon Lett.*, 2021, **31**, 177–199.
30 A. Marinkas, F. Arena, J. Mitzel, G. M. Prinz, A. Heinzel, V. Peinecke and H. Natter, *Carbon*, 2013, **58**, 139–150.
31 B. Chehroudi, *Propellant Combustion: Graphene Science Handbook*, 2016, pp. 391–398.
32 F. Mouhat, F.-X. Coudert and M.-L. Bocquet, *Nat. Commun.*, 2020, **11**, 1566.
33 A. S. Nia and W. H. Binder, *Prog. Polym. Sci.*, 2017, **67**, 48–76.
34 D. R. Dreyer, S. Park, C. W. Bielawski and R. S. Ruoff, *Chem. Soc. Rev.*, 2010, **39**, 228–240.
35 J. Wu, H. Lin, D. J. Moss, K. P. Loh and B. Jia, *Nat. Rev. Chem.*, 2023, **7**, 162–183.
36 V. Brusko, A. Khannanov, A. Rakhmatullin and A. M. Dimiev, *Carbon*, 2024, **229**, 119507.
37 R. Feng, W. Zhou, G. Guan, C. Li, D. Zhang, Y. Xiao, L. Zheng and W. Zhu, *J. Mater. Chem.*, 2012, **22**, 3982–3989.
38 D. R. Dreyer, K. A. Jarvis, P. J. Ferreira and C. W. Bielawski, *Polym. Chem.*, 2012, **3**, 757–766.
39 Y.-J. Ryu, C.-S. Yoo, M. Kim, X. Yong, J. Tse, S. K. Lee and E. J. Kim, *J. Phys. Chem. C*, 2017, **121**, 10078–10086.
40 Y. J. Ryu, C.-S. Yoo, J. Lim, M. Kim, X. Yong and J. S. Tse, *J. Phys. Chem. C*, 2020, **124**, 107–114.
41 S. Fujimori and S. Inoue, *J. Am. Chem. Soc.*, 2022, **144**, 2034–2050.
42 X. Jia, J. Campos-Delgado, M. Terrones, V. Meunier and M. S. Dresselhaus, *Nanoscale*, 2011, **3**, 86–95.
43 A. Lerf, H. He, M. Forster and J. Klinowski, *J. Phys. Chem. B*, 1998, **102**, 4477–4482.
44 L. Martínez, R. Andrade, E. Birgin and J. Martínez, *J. Comput. Chem.*, 2009, **30**, 2157–2164.
45 T. K. Woo, P. M. Margl, P. E. Blöchl and T. Ziegler, *J. Phys. Chem. B*, 1997, **101**, 7877–7880.
46 J. VandeVondele, M. Krack, F. Mohamed, M. Parrinello, T. Chassaing and J. Hutter, *Comput. Phys. Commun.*, 2005, **167**, 103–128.
47 B. G. Lippert and J. H. M. Parrinello, *Mol. Phys.*, 1997, **92**, 477–488.
48 J. VandeVondele and J. Hutter, *J. Chem. Phys.*, 2007, **127**, 114105.
49 M. Born and R. Oppenheimer, in *Quantum Chemistry: Classic Scientific Papers*, World Scientific, 2000, pp. 1–24.
50 S. Grimme, J. Antony, S. Ehrlich and H. Krieg, *J. Chem. Phys.*, 2010, **132**, 154104.
51 G. Bussi, D. Donadio and M. Parrinello, *J. Chem. Phys.*, 2007, **126**, 014101.
52 G. J. Martyna, D. J. Tobias and M. L. Klein, *J. Chem. Phys.*, 1994, **101**(10), 1063.
53 F. Neese, F. Wennmohs, A. Hansen and U. Becker, *Chem. Phys.*, 2009, **356**, 98–109.
54 B. Helmich-Paris, B. de Souza, F. Neese and R. Izsák, *J. Chem. Phys.*, 2021, 155.
55 F. Neese, *J. Comput. Chem.*, 2023, **44**, 381–396.
56 A. D. Becke, *J. Chem. Phys.*, 1992, **96**, 2155–2160.
57 P. J. Stephens, F. J. Devlin, C. F. Chabalowski and M. J. Frisch, *J. Phys. Chem.*, 1994, **98**, 11623–11627.
58 F. Weigend and R. Ahlrichs, *Phys. Chem. Chem. Phys.*, 2005, **7**, 3297–3305.
59 N. Mardirossian and M. Head-Gordon, *J. Chem. Phys.*, 2016, 144.
60 B. Jeziorski, R. Moszynski and K. Szalewicz, *Chem. Rev.*, 1994, **94**, 1887–1930.
61 R. M. Parrish, L. A. Burns, D. G. Smith, A. C. Simmonett, A. E. DePrince III, E. G. Hohenstein, U. Bozkaya, A. Y. Sokolov, R. Di Remigio and R. M. Richard, *J. Chem. Theory Comput.*, 2017, **13**, 3185–3197.
62 T. M. Parker, L. A. Burns, R. M. Parrish, A. G. Ryno and C. D. Sherrill, *J. Chem. Phys.*, 2014, **140**, 094106.
63 T. Lu and F. Chen, *J. Comput. Chem.*, 2012, **33**, 580–592.
64 I. Mayer, *Chem. Phys. Lett.*, 1983, **97**, 270–274.
65 T. Lu and Q. Chen, *Theor. Chem. Acc.*, 2020, **139**, 25.
66 K. Momma and F. Izumi, *J. Appl. Crystallogr.*, 2011, **44**, 1272–1276.
67 W. Humphrey, A. Dalke and K. Schulten, *J. Mol. Graph.*, 1996, **14**, 33–38.
68 C. Bie, J. Yang, X. Zeng, Z. Wang, X. Sun, Z. Yang, J. Yu and X. Zhang, *Small*, 2025, 2411184.
69 X. Li, Z. Peng, C. Jiang, N. Li, J. Zhang, C. Jin and C. Xiao, *Prog. Solid State Chem.*, 2024, **76**, 100491.
70 R. Gutzler and D. F. Perepichka, *J. Am. Chem. Soc.*, 2013, **135**, 16585–16594.
71 J. Gauss and J. F. Stanton, *J. Phys. Chem. A*, 2000, **104**, 2865–2868.
72 N. C. Craig, P. Groner and D. C. McKean, *J. Phys. Chem. A*, 2006, **110**, 7461–7469.